Stability of the Planar Synchronous Full Two-Body Problem–the Approach of Periodic Orbits

Hai-Shuo Wang[a,b,c], Xiaosheng Xin[d], Xiyun Hou[a,b,c], Jinglang Feng[e]

[a] *School of Astronomy and Space Science, Nanjing University, 163 Xianlin Avenue, Nanjing, 210023, China*
[b] *Institute of Space Environment and Astrodynamics, Nanjing University, 163 Xianlin Avenue, Nanjing, 210023, China*
[c] *Key Laboratory of Modern Astronomy and Astrophysics, Nanjing University, 163 Xianlin Avenue, Nanjing, 210023, China*
[d] *Beijing Institute of Tracking and Telecommunications Technology, Beijing, 100000, China*
[e] *Mechanical And Aerospace Engineering, University of Strathclyde, Glasgow, Glasgow, UK*

Abstract

We investigate the dynamical stability of the synchronous state of the planar full two-body problem (PF2BP) by employing the approach of periodic orbit in the primary's body-fixed frame. Our results indicate that the traditional model to the spin-orbit resonances by neglecting the rotational motion's influence on the orbital motion is inappropriate in the binary asteroid system because the two asteroids are close to each other, leading to strong coupling between the orbits and rotations. Focusing on the high-order spin-orbit resonance, the family genealogy of periodic orbits in the unperturbed case is broken apart by some resonances in the perturbed case. In the case of no spin-orbit resonances, the periodic orbit is near-circular and is generally but not always stable. In the case of spin-orbit resonances, the periodic orbit can be elliptic, and one branch of the periodic orbits is stable. In contrast, the other branch is unstable for small to moderate orbit eccentricities.

Keywords: Celestial mechanics, Binary asteroid, Rotational dynamics, Stability, Periodic Orbits

Email addresses: wanghs@smail.nju.edu.cn (Hai-Shuo Wang), houxiyun@nju.edu.cn (Xiyun Hou)

1. Introduction

The Full Two-Body Problem (F2BP), which studies the orbital and rotational motion of two finite rigid bodies under their mutual gravitational potential, is significant in understanding the evolution of binary asteroids and spacecraft dynamics applicable in future asteroid exploration missions. Many works have been done on this topic, such as [1, 2, 3, 4, 5, 6, 7]. These works either presented the fundamental formalism of the problem or identified various stability configurations and criteria in the system. Specific results were also obtained with different simplifications to F2BP. [8] devised robust algorithms for solving relative equilibria for a system with a general mass distribution and a point mass using the Sphere-Restricted Full Two-Body Problem (SRF2BP) model. Relative equilibria and periodic orbits for a planar system composed of an ellipsoid and a sphere are computed by [9]. Stability properties of different equilibrium configurations were analysed in [10] for the planar F2BP (PF2BP) by using a mutual potential truncated the 2nd order.

The knowledge of the full two-body system is fundamental in studying the dynamical evolution of the binary asteroid system, especially the spin-orbit resonance. Usually, the primary is assumed as a sphere, and the spin-orbit coupling of the secondary (or the satellite) is the research focus. This assumption allows the sphere's rotation to be excluded from the system [11]. Moreover, the mutual orbit is usually assumed invariant, i.e., remains uninfluenced by the rotational motions, and only the rotational motion of the secondary is considered. This model is widely used in studying the spin-orbit coupling of a Sun-Planet system or a Planet-Satellite system, such as the Sun-Mercury system [12, 13] or the Saturn-Hyperion system [14]. In these studies, either the Hamiltonian of the rotational motion is expanded to high orders to analyze each spin-orbit resonance term [15, 16], or the numerical tool, surface of Poincaré section, is used to describe the stability of these resonances intuitively [9, 17, 8, 18]. Recently, these studies have been extended to cases where the primary is also not a sphere [7, 19, 20, 21, 22, 23]. In such cases, the spin-spin coupling due to the direct interaction between the non-spherical parts of the two bodies is a new phenomenon that does not exist in the binary system composed of a sphere and an irregular body [24]. However, the assumption in most previous studies that the invariant mutual orbit is no longer valid for the binary asteroid systems, as the two asteroids have closer mutual distance and a higher mass ratio than the Planet-Satellite or the Sun-Planet system. Due to the coupling between the asteroid's rotation and the mutual orbit, more degrees of freedom (DOF) have to be considered, and the method of Poincaré section [1] is hard to to be directly used. Usually there are two approaches to deal with such high DOF systems. One approach is based on averaging of the Hamiltonian. By focusing on some specific resonant term of the Hamiltonian and by removing other short period terms through the averaging process, we are able to reduce the Hamiltonian to a 1-DOF or 2-DOF system. Using the reduced averaged 1-DOF or 2-DOF system, we are able to describe the properties of the phase space near this specific resonance, such as equilibrium configuration, stability, and resonance width. The advantage of this approach is that there are formal ways to do the averaging, and the global properties of the resonance such as the resonance width can be obtained. The disadvantage is that the averaged system cannot accurately reflect the dynamics of the full system due to the fact that in practice the averaging process has to be truncated at finite orders and the fact that averaging process may be inaccurate or even impossible due to the interaction between different resonant terms. The other approach is based on periodic orbits. For complex dynamical systems, the periodic orbits serve as backbone of the phase space. Most of the time they actually also correspond to specific resonances of the system. By studying how they appear in the phase space and how their stability change with the parameters such as the orbit size, we are able to peep the complex dynamics of the system through them. The advantage is that there

[1]It may help to intuitively visualize whether a single orbit is regular or chaotic [20], but generally it doesn't help in separating regular regions from chaotic regions in the phase space for dynamical systems of high dimensions.

are formal ways to compute the periodic orbits and describe their stability. The approach is completely numerical and easy. The disadvantage is that we are only able to know the stability of the periodic orbit itself but are unable to describe to what extend the stable region is for quasi-periodic motions with the same energy level as the periodic orbit. This approach is taken by [25] to study the boundary of the binary asteroid's orbit eccentricity when it is trapped in the synchronous state (i.e. the 1:1 spin-orbit resonance). Continuing the approach of periodic orbits, [26] adopted an averaged ellipsoid-ellipsoid model to study the long-term dynamics of binary asteroids influenced by BYORP, tides, and YORP effect. They pointed out that the secondary's synchronous state may break when the primary crosses these spin-orbit resonances (including some high-order resonances). Naturally, the stability of these high-order resonances is worth studying in the completed ellipsoid-ellipsoid model (i.e. the planar full two-body problem).

In this paper, we will study the stability of the planar full two-body problem (PF2BP) by focusing on the spin-orbit resonance between primary's rotation and orbital motion. Except for the well-established $1:1$ one, another example—the 2:3 spin-orbit resonance—will be emphasized in Section 3 and 4. Different from previous work with the assumption of invariant orbit, we build a mathematical model for the periodic orbit in the PF2BP by simultaneously considering the orbital motion and the body's rotation. (1) The difference between this model and the traditional model is analyzed at first. As a result, there is a contradiction between the full dynamics in [8, 18, 10] and the traditional approach of assuming an invariant mutual orbit. It indicates that the influence on the orbital motion by the rotational motion should be taken into consideration. (2) We compute the periodic orbit first in the unperturbed problem (two spheres orbiting each other), and then in the ellipsoid-sphere system, and then in the ellipsoid-ellipsoid system. By this way, we can observe how the genealogy and stability of periodic families are changed by the non-spherical parts of the two asteroids. (3) At last, as an example of relatively large non-spherical perturbations, two binary asteroid systems, 66391 Moshup and 65803 Didymos, are analyzed with our method.

The paper is organized as follows. Section 2 introduces the equations of motion for the planar full two-body problem (PF2BP). The mutual potential is truncated at the second order. Section 3 revisits the approach of invariant orbit by the numerical tool of Poincaré maps. Two resonances—the 1 : 1 one and the 2 : 3 one are given special attention in order to compare with the PF2BP model. Section 4 presents in detail the approach of periodic orbits, including the computation algorithms, the genealogy of periodic families (including the ones in spin-orbit resonances and the ones not in), and the stability of these periodic orbits. Section 5 concludes the study. Section 6 discusses the dynamical existence of asteroid pairs with an unexpected low-angular momentum.

2. Model Description

The dynamical model used in our work is described in this section. Under the assumption of planar motion and fixed ellipsoidal shapes, we model the two bodies as ellipsoids rotating about their shortest axes, respectively, with mutual orbit coplanar with their equatorial planes. Fig. 1 shows the geometry of the system. $\mathcal{A}$ is the secondary body, which is smaller and in synchronous rotation with its orbit, and $\mathcal{B}$ is the primary body. The coordinate systems $O-XY$ and $O_B - X_BY_B$ are constructed in the body-fixed frame of $\mathcal{A}$ and $\mathcal{B}$, respectively, with origins at the barycentres and coordinate axes pointing along the corresponding longest and intermediate axes of $\mathcal{A}$ and $\mathcal{B}$, respectively. An inertial frame $O'-xy$ is also constructed with the origin O' at the barycentre of the system. The useful variables are: $\boldsymbol{S}$ the position vector of the barycentre of $\mathcal{B}$ relative to that of $\mathcal{A}$, θ and Θ the quadrant angles of $\boldsymbol{S}$ in $O-XY$ and $O'-xy$, respectively, ϕ the rotation angle of $O_B - X_BY_B$ with respect to $O - XY$, θ_A and θ_B the rotation angles of $O - XY$ and $O_B - X_BY_B$ relative to the inertial frame $O' - xy$, respectively. The angles satisfy the equations

$$\Theta = \theta_A + \theta, \quad \theta_B = \theta_A + \phi, \quad \delta = \theta - \phi. \tag{1}$$

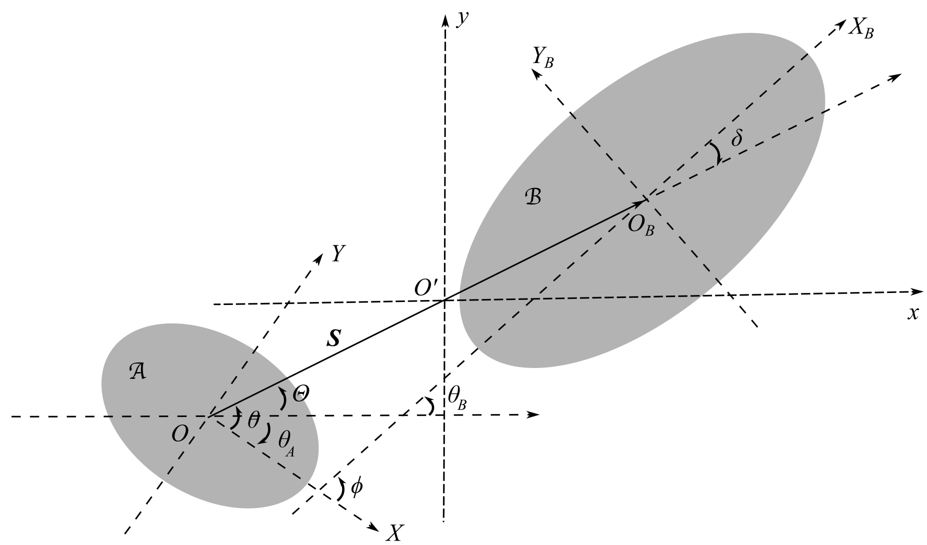

Figure 1: Schematic diagram of the planar F2BP.

The semi-axes and masses of $\mathcal{A}$ and $\mathcal{B}$ are denoted as

$$a_A, b_A, c_A, m_A; \quad a_B, b_B, c_B, m_B. \tag{2}$$

The non-spherical gravity coefficients J_2 and J_{22} of $\mathcal{A}$ and $\mathcal{B}$ are given by [27]

$$J_2^* = \frac{a_*^2 + b_*^2 - 2c_*^2}{10\bar{a}_*^2}, \quad J_{22}^* = \frac{a_*^2 - b_*^2}{20\bar{a}_*^2} \tag{3}$$

in which $*$ represents $\mathcal{A}$ or $\mathcal{B}$ and the reference radius $\bar{a}_*$ is defined as $\bar{a}_* = (a_* b_* c_*)^{1/3}$.

The units adopted in this work are

$$\begin{cases} [M] = m_A + m_B \\ [L] = a \\ [T] = \left([L]^3/G[M]\right)^{1/2} \end{cases} \tag{4}$$

in which a is the mean distance between the barycentres of $\mathcal{A}$ and $\mathcal{B}$ and G is the gravitational constant. According to [23], the mutual potential of $\mathcal{A}$ and $\mathcal{B}$ truncated at 2nd order is

$$U = -m\left[\frac{1}{S} + \frac{1}{S^3}(A_1 + A_2\cos 2\theta + A_3\cos 2\delta)\right], \tag{5}$$

where

$$\begin{aligned}
&S = \|\boldsymbol{S}\|,\ m = \mu(1-\mu),\ \mu = \frac{m_A}{m_A + m_B}, \\
&A_1 = \frac{1}{2}(J_2^A \alpha_A^2 + J_2^B \alpha_B^2),\ A_2 = 3J_{22}^A \alpha_A^2,\ A_3 = 3J_{22}^B \alpha_B^2, \\
&\alpha_* = \bar{a}_*/a.
\end{aligned} \tag{6}$$

This potential is in fact equivalent to the potential in [10] expressed by moments of inertia, only with difference in definition of variables. The mutual potential is inversely proportional to the square of the mutual distance S. The 4th order term $\sim (J_2^*/S^2)^2$ is usually much smaller than the 2nd order term. So the 2nd-order mutual potential dominates. We have to remark that the only purpose of the ellipsoid shape assumption in this work is that the second order mutual potential can be easily calculated with the ellipsoid shape parameters. When truncated at the second-order, the mutual potential does not change with the asteroids' shape as long as they have the same second order gravity coefficients. The figure-figure interaction between the two asteroids, , i.e., the mutual gravity depending on the asteroid's shapes, only appear at the fourth order or even higher of the mutual potential[23]. Usually, unless the two asteroids are very close to each other, the figure-figure interaction is weaker and neglected in the current study. It is worth noting that the increase in the non-spherical terms J_2^* and J_{22}^* or the decrease in the mutual mean distance a could achieve the same effect of increasing the non-spherical potential coefficients A_i, $i = 1, 2, 3$.

Substituting equation (B.1) into the equations of motion (EOMs) of the system [23]

$$\begin{cases}
\ddot{S} = S(\dot{\theta} + \dot{\theta}_A)^2 - \dfrac{1}{m}\dfrac{\partial U}{\partial S} \\
\ddot{\theta} = -2\dfrac{\dot{S}}{S}(\dot{\theta} + \dot{\theta}_A) - \left(\dfrac{1}{I_z^A} + \dfrac{1}{mS^2}\right)\dfrac{\partial U}{\partial \theta} - \dfrac{1}{I_z^A}\dfrac{\partial U}{\partial \phi} \\
\ddot{\phi} = -\dfrac{1}{I_z^A}\dfrac{\partial U}{\partial \theta} - \left(\dfrac{1}{I_z^A} + \dfrac{1}{I_z^B}\right)\dfrac{\partial U}{\partial \phi} \\
\ddot{\theta}_A = \dfrac{1}{I_z^A}\dfrac{\partial U}{\partial \theta} + \dfrac{1}{I_z^A}\dfrac{\partial U}{\partial \phi}
\end{cases} \tag{7}$$

in which

$$I_z^A = \frac{\mu\left(a_A^2 + b_A^2\right)}{5a^2} \text{ and } I_z^B = \frac{(1-\mu)\left(a_B^2 + b_B^2\right)}{5a^2}$$

are the moments of inertia of $\mathcal{A}$ and $\mathcal{B}$ about their axes of rotation, respectively, we have

$$\begin{cases} \ddot{S} = S(\dot{\theta}+\dot{\theta}_A)^2 - \left[\dfrac{1}{S^2} + \dfrac{3}{S^4}(A_1 + A_2\cos 2\theta + A_3\cos 2\delta)\right] \\ \ddot{\theta} = -2\dfrac{\dot{S}}{S}(\dot{\theta}+\dot{\theta}_A) - \dfrac{2}{S^5}(A_2\sin 2\theta + A_3\sin 2\delta) - \dfrac{2mA_2}{I_z^A}\dfrac{\sin 2\theta}{S^3} \\ \ddot{\phi} = \dfrac{2mA_3}{I_z^B}\dfrac{\sin 2\delta}{S^3} - \dfrac{2mA_2}{I_z^A}\dfrac{\sin 2\theta}{S^3} \\ \ddot{\theta}_A = \dfrac{2mA_2}{I_z^A}\dfrac{\sin 2\theta}{S^3} \end{cases}. \tag{8}$$

Equation (8) is the full EOMs for the PF2BP under mutual potential truncated at 2nd order.

3. The approach of Invariant Orbit

Poincaré map is usually employed to analyze the dynamics of spin-orbit resonances, such as [14] for studying the rotation of Hyperion and [20] for analysing the spin-orbit coupling of binary asteroid. Other methods for the study of spin-orbit coupling are also available from the literature including the SONYR model applied to Mercury [28], Lie-Poisson numerical integration algorithms with visualisation aided by MEGNO maps [29], etc. Before we present our results by periodic orbit approach which considers the full dynamics of the PF2BP in the next section, in this section, we use Poincaré maps to show the results of traditional approach by assuming an invariant mutual orbit for the two rigid bodies. The reason why we include this section is to compare the results with following results via the approach of periodic orbits.

To be parallel with previous works, $\mathcal{A}$ is assumed to be a sphere rotating with an arbitrary angular velocity ω_A, rending its rotational motion completely decoupled from its orbital motion. Thus we only need to consider the spin-coupling of $\mathcal{B}$. When $\mathcal{A}$ is much larger than $\mathcal{B}$, it is the case studied in previous works, usually for the Sun-planet system or the planet-satellite system. The mutual orbit is approximated as a two-body Keplerian orbit, i.e., $S = (1-e^2)/(1+e\cos f)$ in which e is the orbit eccentricity and f is the true anomaly relative to the inertial frame. The rotational motion of $\mathcal{B}$ satisfies

$$\ddot{\phi} = \frac{2mA_3}{I_z^B}\frac{\sin 2\delta}{S^3} \tag{9}$$

which is obtained from the third equation in equation (8) by letting $A_2 = 0$. δ is related to ϕ via $\delta = \theta - \phi = f - \omega_A t - \phi$. The Poincaré map is obtained by plotting $\dot{\delta}_p$ against ϕ_p in which p indicates that the values are taken at the pericenter of the mutual orbit. Note that according to equation (1) $\dot{\delta}$ is obtained from $\dot{\delta} = \dot{\theta} - \dot{\phi}$. Moreover, since $\dot{\delta} = \dot{\Theta} - \dot{\theta}_B$ also satisfies, the locations of spin-orbit resonances $n : \omega_B = p : q$, where $n = \left\langle \dot{\Theta} \right\rangle$, $\omega_B = \left\langle \dot{\theta}_B \right\rangle$ and $\langle . \rangle$ indicates values averaged over one orbit, can be easily detected on the Poincaré map. We call the spin-orbit resonance with $p/q > 1$ sub-critical and that with $p/q < 1$ super-critical. n always equals unity due to our choice of unit system. Because of the symmetry of the mutual potential truncated at 2nd order, ϕ_p is equivalent to $\phi_p + \pi$. Therefore, ϕ_p is restricted to the interval from 0 to π.

Two cases are studied and the system parameters for each case are listed in Table 1. The parameters are chosen such that A_3 in equation (9) and mass ratio between the secondary and the primary keeps unchanged between these two cases. Case #1 is for a system with $\mathcal{A}$ as the larger component, which is the model adopted for the Sun-Mercury system [28] or Saturn-Hyperion system [14]. Case #2 is representative of a system with $\mathcal{A}$ as the smaller component, which is the model studied in [8, 18]. The Poincaré map for the two cases are shown in Fig. 2. ~~The orbit eccentricities for both cases are taken to be $e = 0.1$.~~ In the following, we will focus on two spin-orbit resonances—the $1:1$ one and the $2:3$ one. The 0th-order resonance (1:1 resonance) is the primary resonance. The 1st-order resonances have some obvious bifurcations and stability transitions, which will be discussed later. Bifurcations only occur at the 1st-order resonances, but not at everyone. Some resonances with small values (such as 6:7, 5:6) approach the 1:1 one, indicating they are easier to overlap with each and cause chaos in the perturbed case. The resonance with a large value (such as 1:2 resonance) is too weak so that it can be easily crossed without bifurcation. Therefore, the 1:1 and 2:3 resonances are ideal examples to find out dynamic details.

3.1. 1 : 1 *resonance*

It is clear from Fig. 2(a) that the resonance centres of the 1 : 1 resonance for Case #1 are at $\phi_p = 0$ and $\phi_p = \pi$, which indicates that the stable configuration of this resonance corresponds to the long-axis mode as depicted in Fig. 3. It seems that Case #1 matches the model for the widespread scenario in our solar system, such as our Earth-Moon system and the Pluto-Charon system, and the results agree with each other. However, according to [10] who analysed the full system instead of just the rotational motion, for the long-axis mode, there exists a minimum distance a_c between the two bodies below which this configuration is unstable (see equation (76) in [10]). a_c for this case is calculated to be ~ 9000 m which is larger than the mutual distance $a = 3000$ m. Therefore, the long-axis mode configuration of 1 : 1 resonance for Case #1 is actually unstable, which contradicts that shown in Fig. 2(a). Numerical simulation of the system considering the full dynamics also supports this conclusion. The main reason behind this contradiction is that the distance between the two bodies in Case #1 is so small that the coupling of the rotational and orbital motion is very strong, which makes the approach of invariant orbit invalid.

According to Fig. 2(b), for Case #2 the stable configuration for the 1 : 1 resonance should also be the long-axis mode. However, according to [8, 18, 10] who analysed the full system instead of just the rotational motion, for a small sphere and a large ellipsoid which are close to each other, the long-axis mode is usually the unstable configuration. a_c for this case is calculated also to be ~ 9000 m which is greater than the mutual distance $a = 3000$ m. Our numerical exploration for this resonance by considering the full dynamics of Case #2 does find that this configuration is unstable. The obvious contradiction with Fig. 2(b) again indicates that the assumption for an invariant mutual orbit in Case #2 may be insufficient for even qualitatively describing the system.

3.2. 2 : 3 *resonance*

For the 2 : 3 resonances, according to Fig. 2, the resonance centres are also at $\phi_p = 0$ and $\phi_p = \pi$ for both cases. This indicates that the stable configuration

Table 1: System parameters adopted for the PSR2BP.

		Case #1	Case #2
$\mathcal{A}$	a_A	1500 m	500 m
	b_A	1500 m	500 m
	c_A	1500 m	500 m
	Density	2.0 g cm^{-3}	2.0 g cm^{-3}
$\mathcal{B}$	a_B	500 m	1500 m
	b_B	480 m	1493 m
	c_B	480 m	1493 m
	Density	2.0 g cm^{-3}	2.2 g cm^{-3}
Mass ratio		$m_B/m_A = 0.034$	$m_A/m_B = 0.034$
Semimajor axis	a	3000 m	3000 m
~~Eccentricity~~	$\cancel{e}$	~~0.1~~	~~0.1~~

for this resonance is the long-axis mode when the system is located at the pericenter of their mutual orbit. For Case #1, this conclusion agrees with the real world (for example, the Sun-Mercury system). However, for Case #2, we will show in the following (see Section 4.3) that the true stable configuration by considering the full dynamics is not the long-axis mode but the short-axis mode. This again indicates that the assumption for an invariant mutual orbit in Case #2 may be insufficient for even qualitatively describing the system.

From the two examples above, we know that there is a contradiction between the results of the full dynamics of the PF2BP and the results by the traditional approach of assuming an invariant mutual orbit. This indicates that the influence on the orbital motion by the rotational motion should be taken into consideration when dealing with the spin-orbit coupling problem in the binary asteroid system. If we have to simultaneously consider the orbital motion and the rotational motions of the two asteroids, the DoF of the system is 4. Poincaré map is no-longer a valid tool for such a system. In the following we abandon this approach and focus on the approach of periodic orbits, which is

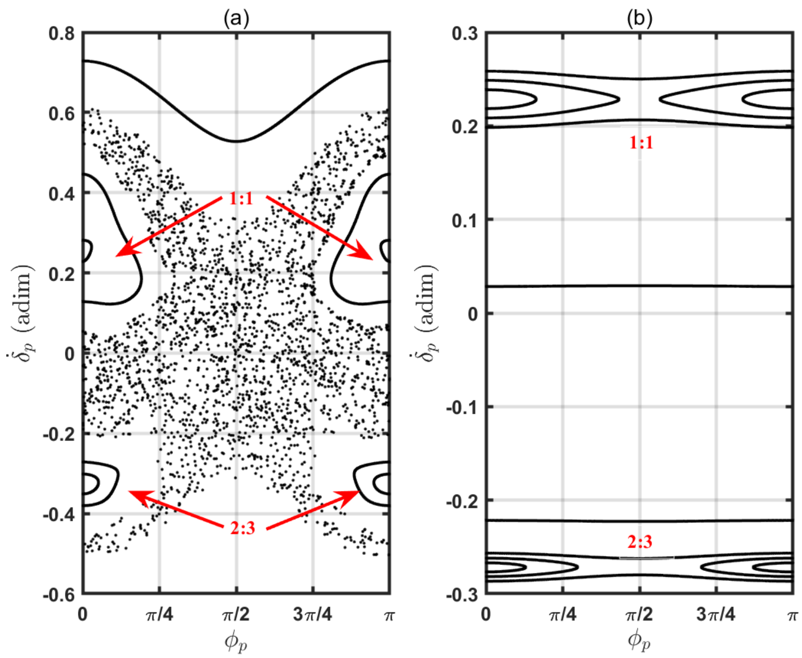

Figure 2: The Poincaré maps for two sphere-ellipsoid systems. The orbit eccentricities when generating these maps is $e = 0.1$. The locations of spin-orbit resonances are indicated by the red arrows. (a) Case #1; (b) Case #2.

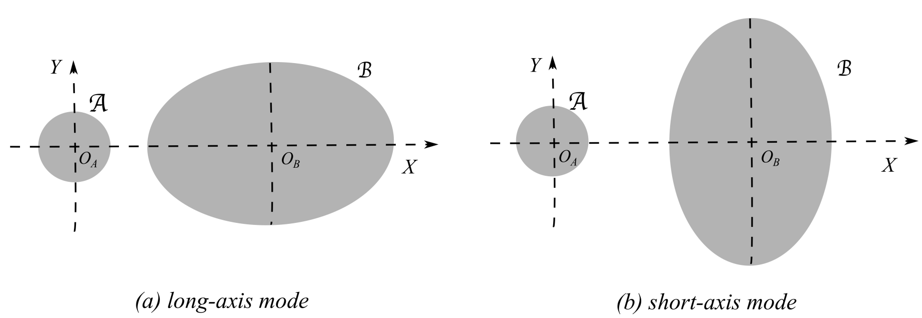

Figure 3: Two 1:1 spin-resonance configuration of the sphere-ellipsoid system. The long-axis mode and short-axis mode denote the configurations where the long axis and short axis of $\mathcal{B}$ point towards the centre of $\mathcal{A}$, respectively.

seldom seen in literature on this problem and is the focus of the current study.

4. The approach of periodic orbits

4.1. Dynamical Substitutes

In the PF2BP composed of an ellipsoidal $\mathcal{A}$ which rotates synchronously with its orbit and a sphere $\mathcal{B}$, there are two types of equilibrium states in the body-fixed frame of $\mathcal{A}$ for $\mathcal{B}$, as depicted in Fig. 4 where $\mathcal{B}$ is located at the equilibria [18]. However, if $\mathcal{B}$ is not a sphere, the equilibria usually do not exist and the location of $\mathcal{B}$ is no longer fixed [30] in the body-fixed frame of $\mathcal{A}$. Due to the addition of one external frequency $\omega_B - 1$ [2] in the body-fixed frame of $\mathcal{A}$ which is introduced by the relative rotation of $\mathcal{B}$'s non-spherical part with respect to $\mathcal{A}$, a special periodic solution for the orbital motion of $\mathcal{B}$ in the body fixed frame of $\mathcal{A}$ with orbit period $T = 2\pi/|\omega_B - 1|$ can be obtained. This periodic orbit can be viewed as forced periodic motions of $\mathcal{B}$ by the periodic movement of its non-spherical part. In this study, we name it as dynamical substitute after [30] and [31], originating from some other similar dynamical structures related to the Restricted Three-Body Problem [32, 33, 34]. These dynamical substitutes are exactly the periodic orbits we focus in the current work.

Generally, periodic orbits in dynamical systems should satisfy

$$\boldsymbol{X}(T) = \boldsymbol{X}_0, \tag{10}$$

[2]Denote $\mathcal{A}$'s rotation frequency as ω_A, $\mathcal{B}$'s rotation frequency as ω_B, and the orbital frequency as ω_o. In $\mathcal{A}$'s body-fixed frame, there are two basic frequencies of $\mathcal{B}$'s relative motion with respect to $\mathcal{A}$. One is $\omega_o - \omega_A$, and the other is $\omega_B - \omega_A$. Since in our study $\mathcal{A}$ is in synchronous rotation with the orbit, $\omega_A = \omega_o$ and the former frequency disappears. In the units of equation 4, $\omega_o = \omega_A = 1$. As a result, the latter frequency becomes $\omega_B - 1$. One remark is, if $\mathcal{A}$ is not in a synchronous rotation state, then periodic orbits studied in this work should be replaced with quasi-periodic orbits with two basic frequencies $\omega_o - \omega_A$ and $\omega_B - \omega_A$ which are harder to get numerically. Lucky for us, synchronous binary systems are common in the population of binary asteroid systems, which makes the study in the current paper have practical applications to these binary asteroid systems

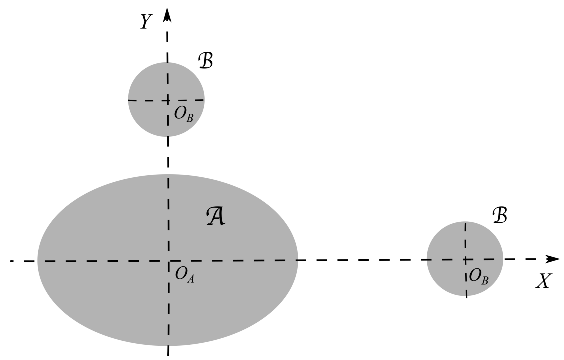

Figure 4: Two types of equilibrium states for the SRF2BP. The spherical $\mathcal{B}$ is located at the relative equilibria of the ellipsoidal $\mathcal{A}$. Different from Fig. 3, now $\mathcal{A}$ is the ellipsoid and $\mathcal{B}$ is the sphere.

where $\boldsymbol{X}$ is the state vector, $\boldsymbol{X}_0$ denotes the initial state and $\boldsymbol{X}(T)$ is the state after one orbit period T. In our case for the PF2BP, $\boldsymbol{X} = (S, \theta, \phi, \theta_A, \dot{S}, \dot{\theta}, \dot{\phi}, \dot{\theta}_A)^T$ is an eight dimensional vector. The exact form of equation (10) is

$$\begin{cases} S(T) = S_0 \\ \theta(T) = \theta_0 \\ \mathrm{mod}\,(\phi(T), 2\pi) = \phi_0 \\ \mathrm{mod}\,(\theta_A(2\pi), 2\pi) = (\theta_A)_0 \\ \dot{S}(T) = \dot{S}_0 \\ \dot{\theta}(T) = \dot{\theta}_0 \\ \dot{\phi}(T) = \dot{\phi}_0 \\ \dot{\theta}_A(T) = \left(\dot{\theta}_A\right)_0 \end{cases}, \tag{11}$$

where mod is the modulo operator. The fourth equation in equation (11) deserves special notice. Here $\theta_A(2\pi)$ denotes the value of θ_A taken after an integration time of 2π instead of the orbit period T. Recall that the orbital period of the system is 2π under the units in equation (4). Since $\mathcal{A}$ is in synchronous rotation, this requires that the relative geometry of $\mathcal{A}$ repeats after one orbital period 2π. Judging from equation (8), an obvious fact is that θ_A is absent from the EOMs. So equation (8) is actually a 7-dimensional dynamical system. Here,

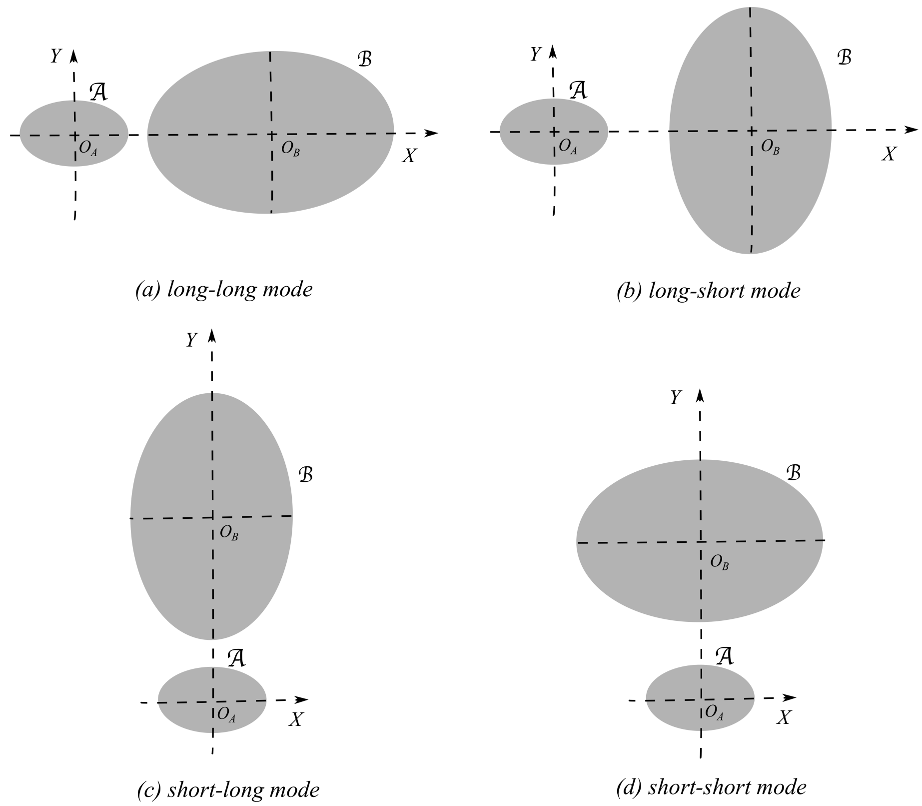

Figure 5: Four configurations of the ellipsoid-ellipsoid system in the PSF2BP. The long-long mode and long-short mode denote the configurations where the long axis and short axis of $\mathcal{B}$ align with the long axis of $\mathcal{A}$, respectively. The short-long mode and short-short mode denote the configurations where the long axis and short axis of $\mathcal{B}$ align with the short axis of $\mathcal{A}$, respectively.

θ_A is added into the variable list not only to ensure that $\mathcal{A}$ is in synchronous rotation with its orbit, but also to construct an 8-dimensional Hamiltonian system so that the symplectic structures of the Hamiltonian system can be utilized (e.g., the eigenvalues appear in pair).

Equation (11) can be numerically solved with iterations starting from an initial guess. Due to symmetry of the mutual potential truncated at 2nd order (equation (B.1)), four possible initial state configurations are allowed as shown in Fig. 5. Also due to the symmetry, equation (11) can be reduced to

$$\begin{cases} \theta(T/2) = 0 \\ \phi(T/2) = \phi_0 + \mathrm{sgn}(\omega_B - 1) \cdot \pi \\ \theta_A(\pi) = \pi \\ \dot{S}(T/2) = 0 \end{cases} \tag{12}$$

for the long-long/long-short modes and

$$\begin{cases} \theta(T/2) = \pi/2 \\ \phi(T/2) = \phi_0 + \mathrm{sgn}(\omega_B - 1) \cdot \pi \\ \theta_A(\pi) = \pi \\ \dot{S}(T/2) = 0 \end{cases}, \tag{13}$$

for the short-long/short-short modes, where sgn is the sign function, and θ, ϕ, θ_A and $\dot{S}$ are all functions of variables S_0, $\dot{\theta}_0$, $\dot{\phi}_0$ and $\left(\dot{\theta}_A\right)_0$ which are numerically corrected from their initial guesses to satisfy equation (12) or (13).

For the simplest case when $\mathcal{B}$ is a sphere, its orbit in the body-fixed frame of $\mathcal{A}$ is a fixed point. The rotational and orbital motion of $\mathcal{B}$ is decoupled and initial guesses can be taken as

$$S_0 = 1,\ \left(\theta_A\right)_0 = 0,\ \dot{S}_0 = 0,\ \dot{\theta}_0 = 0,\ \dot{\phi}_0 = \omega_B - 1,\ \left(\dot{\theta}_A\right)_0 = 1$$

and

$$\begin{cases} \theta_0 = 0,\ \phi_0 = 0 \quad long - long \quad mode \\ \theta_0 = 0,\ \phi_0 = \pi/2 \quad long - short \quad mode \\ \theta_0 = \pi/2,\ \phi_0 = \pi/2 \quad short - long \quad mode \\ \theta_0 = \pi/2,\ \phi_0 = 0 \quad short - short \quad mode \end{cases} \tag{14}$$

which can be iterated to solve for the true initial state. Equation (14) is still a good approximation for the initial guess when the non-spherical terms of $\mathcal{B}$ are relatively small. As the non-spherical terms of $\mathcal{B}$ grow larger, the numerical correction process no longer converges if equation (14) is still used as the initial guess. A parameter $\epsilon \in [0, 1]$ is then introduced together with ϵJ_2^B and ϵJ_{22}^B, and equation (12) or (13) is numerically solved starting from $\epsilon = 0$, which obviously corresponds to the case of a spherical $\mathcal{B}$, and gradually increasing ϵ until it reaches unity. Once a periodic orbit is obtained, periodic orbits belonging to the same family can also be computed through a continuation method with either T or S_0 as the continuation parameter.

The stability of the periodic orbit is determined from the eigenvalues of its associated monodromy matrix, which is obtained from the state transition matrix (STM) $\Phi_{8\times8}$ mapped over one period T, denoted as $\Phi_{8\times8}(T)$. $\Phi_{8\times8}$ is computed from the differential equation

$$\dot{\Phi}_{8\times8} = A_{8\times8}\Phi_{8\times8}, \tag{15}$$

where the matrix $A_{8\times8}$ can be obtained analytically from equation (8). There are always two pairs of eigenvalues equal to 1 (see Appendix Appendix A for more details). The other two pairs λ_i, $i = 1, 2, 3, 4$, are essential to the stability of the periodic orbits. For stable periodic orbits the modulus of all these eigenvalues should be equal to unity, while for unstable ones the modulus of at least one eigenvalue should be greater than one.

4.2. Unperturbed Case — the sphere-sphere model

To better understand the results of the perturbed case, we start with the unperturbed case where $\mathcal{A}$ and $\mathcal{B}$ are both spheres. In the unperturbed case, the orbital motion and the rotational motions are completely decoupled from each other. $\mathcal{A}$ and $\mathcal{B}$ have constant angular rotation rates $\dot{\theta}_A = n = 1$ and $\dot{\theta}_B = \omega_B$. As an example, the following system is chosen. The mean distance between the two bodies is $a = 3000$ m. For the body $\mathcal{A}$, $a_A = b_A = c_A = 500$ m. For the body $\mathcal{B}$, $a_B = b_B = c_B = 1000$ m. Since the orbital motion is decoupled from the rotational motion, if $\mathcal{B}$ is on a circular orbit around $\mathcal{A}$, in $\mathcal{A}$'s body-fixed frame $\mathcal{B}$'s trajectory is always a fixed point. After a period of $2\pi/|\omega_B - 1|$, $\mathcal{B}$'s rotation with respect to $\mathcal{A}$'s body-fixed frame repeats. Following Poincaré, we call this family as periodic family of the first kind or simply as near-circular family. On the other hand, if $\mathcal{B}$'s orbit around $\mathcal{A}$ is an elliptic orbit, in order to both the rotational motion and orbital motion to repeat in $\mathcal{A}$'s body-fixed

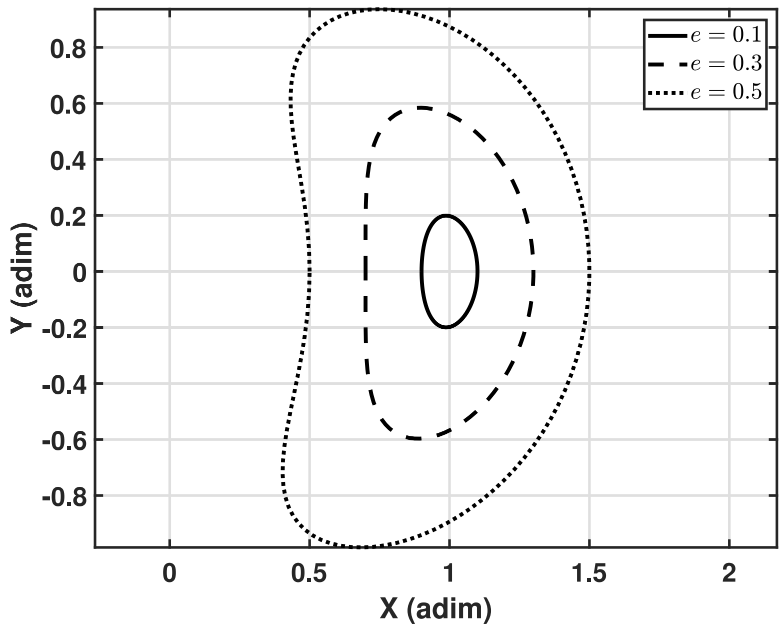

Figure 6: Periodic orbits of spherical $\mathcal{B}$ with different eccentricities shown in the body-fixed frame of spherical $\mathcal{A}$.

frame, $\mathcal{B}$'s rotational frequency should be rational with the orbital frequency. In the inertial frame, the mutual orbit can be an elliptic orbit. During the period $2p\pi$, the orbit (also $\mathcal{A}$) rotates p times and $\mathcal{B}$ rotates q times. In the body-fixed frame of $\mathcal{A}$, $\mathcal{B}$'s relative rotation angle with respect to $\mathcal{A}$ is $2(q-p)\pi$. Since $\mathcal{B}$'s trajectory in the inertial frame is an elliptic orbit, its trajectory in the body-fixed frame of $\mathcal{A}$ is no longer a fixed point, but has a shape as shown in Fig. 6. We call this kind of period family as "periodic family of the second kind" or simply as "resonance family" in this work. In the current study, we only deal with the first order spin-orbit resonances, that is $q-p=\pm 1$.

An innovative $H-\omega_B$ ($\omega_A \equiv 1$) plot is given to show the genealogy between these two kinds of periodic families, as shown by Fig. 7. H is the total angular momentum of the system, and is computed by

$$H_{\text{unperturbed}} = m\sqrt{1-e^2} + I_z^A\dot{\theta}_A + I_z^B\dot{\theta}_B, \tag{16}$$

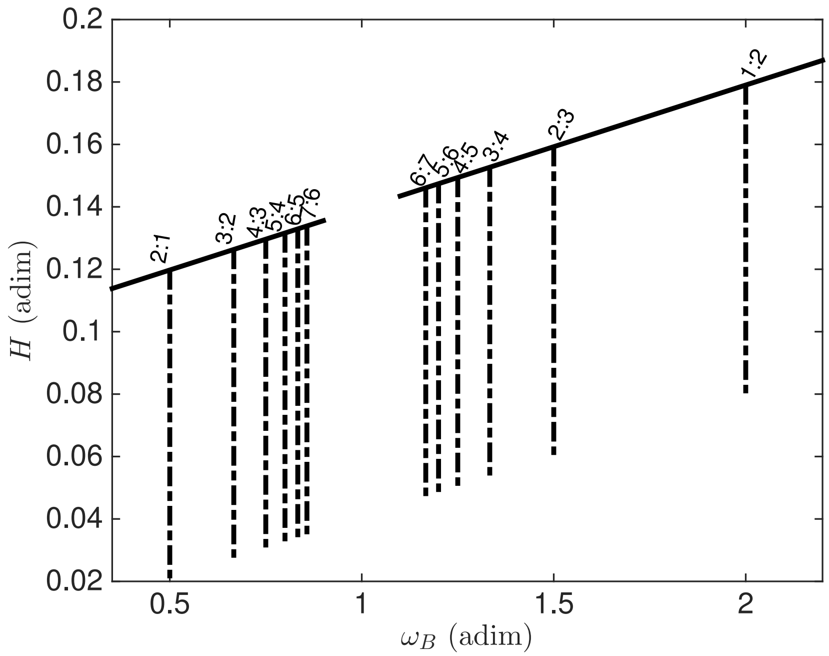

Figure 7: The $H-\omega_B$ curve for an unperturbed system comprised of two spheres with radius 1000 m and 500 m, respectively. The mean mutual distance $a = 3000$ m and eccentricity $e = 0.1$. The dashed lines bifurcate from the solid lines where the resonances occur as the annotations $n : \omega_B$ indicate.

where m is given in equation (6) and e is the orbit eccentricity. In the absence of spin-orbit resonances, $e = 0$. Since ω_B is fixed in the presence of spin-orbit resonances, the $H - \omega_B$ curves for the resonance families appear as dashed vertical lines in Fig. 7. The genealogy between the two families is obvious in Fig. 7—the resonance families bifurcate from the near-circular family at the spin-orbit resonances. The accumulation of first order resonances when they approach the $1:1$ one, indicates that it is much easier for them to overlap with each and cause chaos in the perturbed case, which is already widely reported by many previous studies. In the following, we will add non-spherical terms to $\mathcal{A}$ and $\mathcal{B}$ to observe how the family genealogy changes.

4.3. Perturbed Case — the sphere-ellipsoid model

Before we present our main results where $\mathcal{A}$ and $\mathcal{B}$ both have non-spherical parts, to compare with the results by the approach of invariant orbit in Section 3.2, we first make a short study on the the sphere-ellipsoid model where $\mathcal{A}$ is a sphere. In this case, since $\mathcal{A}$'s rotational motion is decoupled from the system, both the state variables θ_A and $\dot{\theta}_A$ can be ignored in the computation of periodic orbits. For comparison with Section 3, we use the parameters of Case #1 and Case #2 listed in Table 1 as examples. We compute the periodic orbits of the system with varying ω_B. Similar to Section 4.2, the $H-\omega_B$ curves are obtained with each point on the curve representing a periodic orbit. The magnitude of the total angular momentum of the system H is

$$H = I_z\dot{\theta}_A + I_z^B\dot{\phi} + mS^2\dot{\theta} \tag{17}$$

in which $I_z = I_z^A + I_z^B + mS^2$.

A portion of the $H-\omega_B$ curves near the $2:3$ spin-orbit resonance is shown in Fig. 8. Comparing Fig. 8 with Fig. 7, one obvious feature is that the near-circular family is broken apart by the $2:3$ resonance. More detailed analysis of the $H-\omega_B$ curve will be given in the following sections. The focus of the current subsection is to compare the results of our periodic orbit approach which considers the full dynamics with those in Section 3.2. Four example periodic orbits annotated in Fig. 8 are shown in Fig. 9. X and Y are coordinates in $O-XY$, the body-fixed frame of $\mathcal{A}$, and $X = S\cos\theta$, $Y = S\sin\theta$ (the same definition applies in the following similar figures). In Fig. 9 (a),(c), the configuration of the 2:3 spin-resonance orbit is with $\mathcal{B}$'s long axis pointing at $\mathcal{A}$ at the pericenter and with $\mathcal{B}$'s short axis pointing at $\mathcal{A}$ at the apocenter. In Fig. 9 (a),(c), the configuration is contrary.

For Case #1, the periodic orbit with the long-axis mode at the pericenter is stable while that with the short-axis mode at the pericenter is unstable for the $2:3$ spin-orbit resonance, which agrees with Fig. 2(a). However, for Case #2 the periodic orbit with the long-axis mode at the pericenter becomes

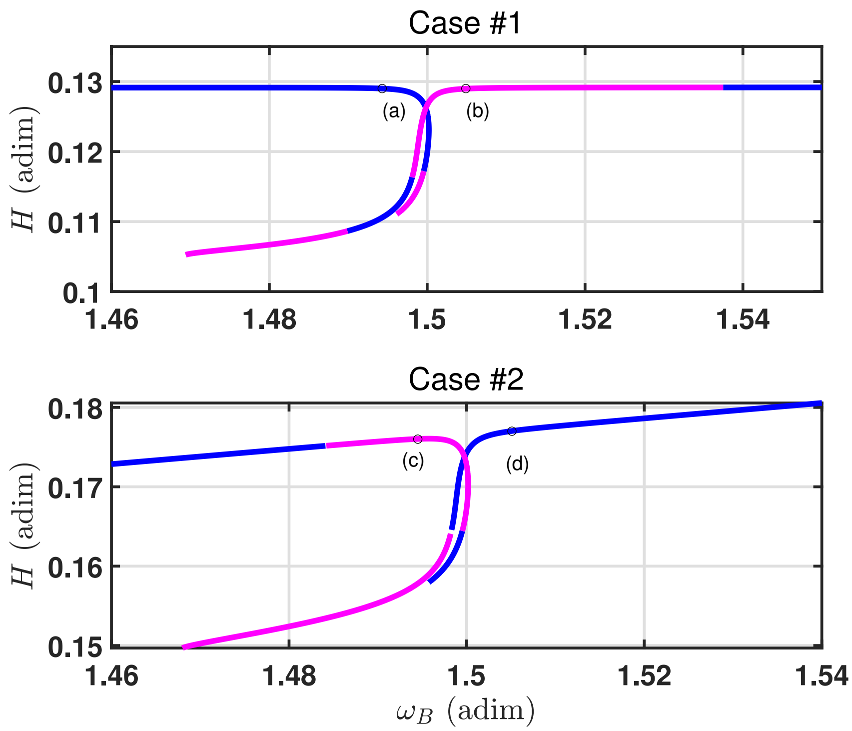

Figure 8: The $H-\omega_B$ curve near the $2:3$ spin-orbit resonance for the sphere-ellipsoid systems. The parameters of the systems are the same as those adopted for Fig. 2. The blue (magenta) lines indicate that the corresponding periodic orbits are stable (unstable). The black circles indicate the locations on the $H-\omega_B$ curve of the corresponding periodic orbits in Fig. 9.

unstable while that with the short-axis mode at the pericenter is stable. This is contradictory to the results shown in Fig. 2(b). Since we have considered the full dynamics in the approach of periodic orbits, we believe the results in Fig. 8 are right. To further verify the stability property of the orbits shown in Fig. 8 (c)∼(d), Fig. 10 and Fig. 11 shows the results by integrating the two initial conditions for 100 orbital periods. For the $2:3$ spin-orbit resonance, according to the d'Alembert relation, the resonance angle should be $2\Theta - 2\theta_B + M$ in which M is the mean anomaly of the mutual orbit.

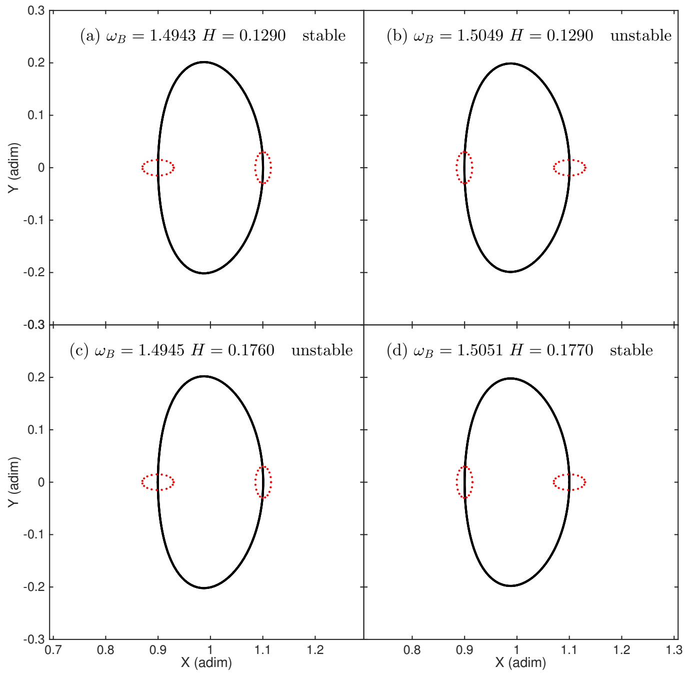

Figure 9: Periodic orbits of 2 : 3 spin-orbit resonance corresponding to (a)∼(d) indicated in Fig. 8. The red dotted ellipsoids show the orientations of $\mathcal{B}$ at pericenter and apocenter.

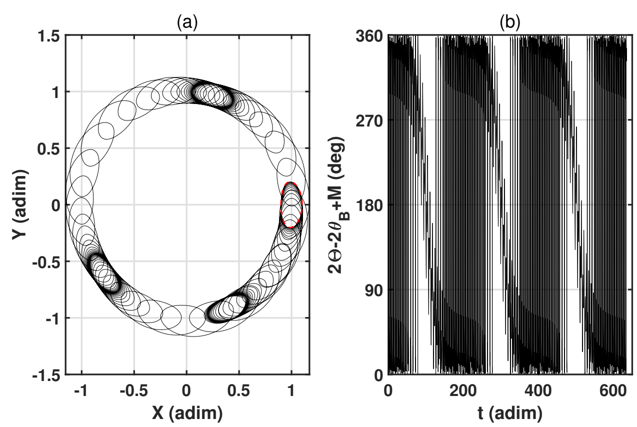

Figure 10: Instability of periodic orbit in Fig. 9(c). (a) red line: original periodic orbit; black line: integrated trajectory for the time span of 100 orbit periods of the original periodic orbit with deviation of 10^{-4} in initial x component. (b) time history of the resonance angle $2\Theta - 2\theta_B + M$.

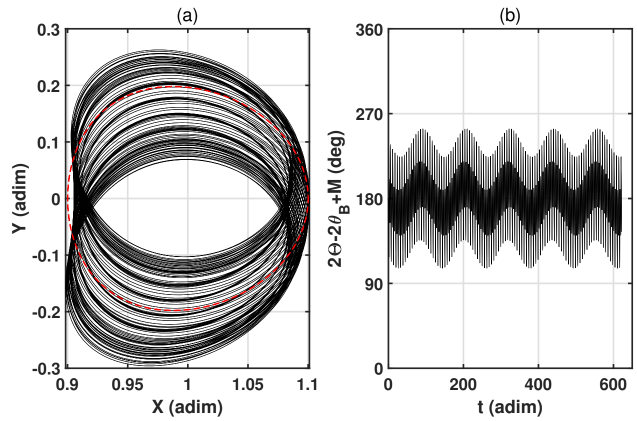

Figure 11: Stability periodic orbit in Fig. 9(d). (a) red line: original periodic orbit; black line: integrated trajectory for the time span of 100 orbit periods of the original periodic orbit with deviation of 10^{-3} in initial x component. (b) time history of the resonance angle $2\Theta-2\theta_B+M$.

4.4. Small Perturbed Case — the ellipsoid-ellipsoid model

This section deals with the case where both $\mathcal{A}$ and $\mathcal{B}$ have small non-spherical terms. The system parameters are $a_B = 1000$ m, $b_B = 960$ m, $c_B = 960$ m and $a_A = 500$ m, $b_A = 480$ m, $c_A = 480$ m, respectively. Their mutual mean distance is $a = 3000$ m. The magnitude of the total angular momentum of the system can also be obtained from equation (17). Intensive numerical computations indicate that periodic orbits corresponding to the short-long and short-short modes in Fig. 5 are generally unstable. Therefore, we mainly focus on the long-long and long-short modes. The $H-\omega_B$ curve is shown in Fig. 12.

Comparison between Fig. 12 and Fig. 7 shows following differences.

(1) The near-circular family in Fig. 7 is broken apart into pieces at the first order spin-orbit resonances. These spin-orbit resonance families join with these pieces to form a series of new periodic families. Actually, the same phenomenon appears in Section 4.3 where we only focus on the 2 : 3 resonance. The breakup does not happen for every first-order resonances but only at every other first-order resonances, such as 2 : 3, 4 : 5 and 6 : 7 for the super-critical resonances and 2 : 1, 4 : 3 and 6 : 5 for the sub-critical resonances.

(2) The resonance family shown in Fig. 7 splits into two branches in the

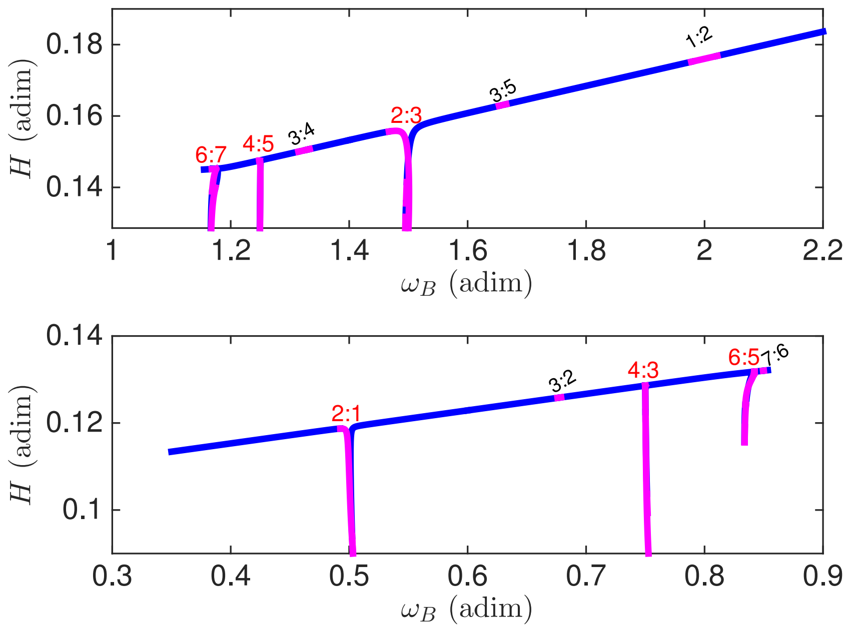

Figure 12: The $H - \omega_B$ curve for a system comprised of an ellipsoidal primary $\mathcal{B}$ with $a_B = 1000$ m, $b_B = 960$ m, $c_B = 960$ m and an ellipsoidal secondary $\mathcal{A}$ with $a_A = 500$ m, $b_A = 480$ m, $c_A = 480$ m, respectively. The mean mutual distance $a = 3000$ m. The blue and magenta lines indicate that the corresponding periodic orbits are stable and unstable, respectively.

perturbed case. Each branch has a different spin-orbit resonance configuration, as already shown in Fig. 8. Take the 2 : 3 again and the 4 : 5 as examples, Fig. 14 and Fig. 15 shows the spin-orbit resonance orbits denoted as black circles in Fig. 13. Periodic orbits in the top (bottom) panels belong to the right (left) branches. As the total angular momentum decreases, the orbit amplitude increases, indicating the eccentricity of the mutual orbit increases. For small to moderate orbit eccentricities, one branch (or configuration) of the spin-orbit resonance is stable while the other branch (or configuration) is unstable. For large orbit eccentricities, both branches become unstable.

(3) Periodic orbits in the near-circular family can also become unstable at other first-order spin-orbit resonances, though the breakup phenomenon does not occur, such as the 3 : 4, 3 : 5 and 1 : 2 resonances in the upper frame and the 3 : 2 and 7 : 6 resonances in the lower frame of Fig. 12.

4.5. Large Perturbed Case — the ellipsoid-ellipsoid model

We take the binary asteroid system 66391 Moshup and 65803 Didymos as examples to illustrate the case with relatively large non-spherical terms. This system is comprised of a primary with rotation axis nearly normal to the orbit plane and a secondary rotating synchronously around the primary [35, 36], which can be well modelled by the ellipsoid-ellipsoid model. The parameters we adopt for the system are listed in Table 2. We obtain the periodic orbits of the system with varying ω_B and plot the $H - \omega_B$ curve shown in Fig. 16. Considering the fact that $\mathcal{B}$ rotates faster than the orbital motion, only the super-critical resonances are given in this case. It showes that the 66391 Moshup and the 65803 Didymos will break when they cross 2:3 spin-orbit resonance.

Compared with the unperturbed case in Fig. 7, the $H - \omega_B$ curve in Fig. 16 is obviously twisted at the resonances, and the twist becomes more severe as the resonance approaches the 1 : 1 resonance. Besides, the first-order resonance families generally become unstable. When the system approaches these resonances, chaotic orbital and rotational motion of $\mathcal{B}$ could be incurred, as an example for the 2 : 3 spin-orbit resonance shows in Fig. 17.

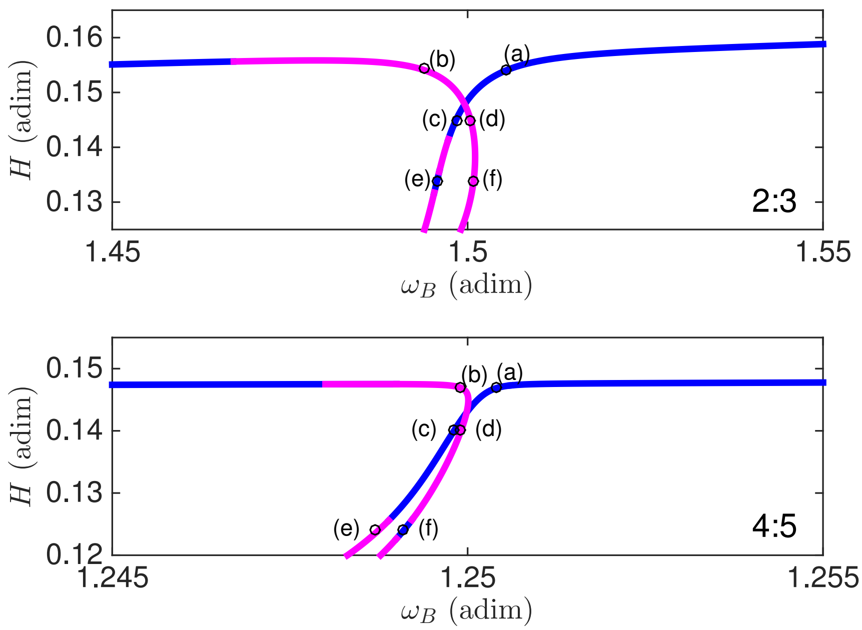

Figure 13: The detailed $H - \omega_B$ curves near 2 : 3 and 4 : 5 spin-orbit resonances. The blue and magenta lines indicate that the corresponding periodic orbits are stable and unstable, respectively. The black circles indicate the locations on the $H-\omega_B$ curve of the corresponding periodic orbits in Fig. 14 and Fig. 15.

Table 2: System parameters for 66391 Moshup adapted from [35] and 65803 Didymos adapted from [37].

		1999KW4	Didymos
$\mathcal{A}$	a_A	297.5 m	103.0m
	b_A	225.0 m	79.0 m
	c_A	171.5 m	66.0 m
	Density	2.81 g cm^{-3}	2.0 g cm^{-3}
$\mathcal{B}$	a_B	708.5 m	399.0 m
	b_B	680.5 m	392.0 m
	c_B	591.5 m	380.0 m
	Density	1.97 g cm^{-3}	2.0 g cm^{-3}
Semimajor axis	a	2548 m	1180 m

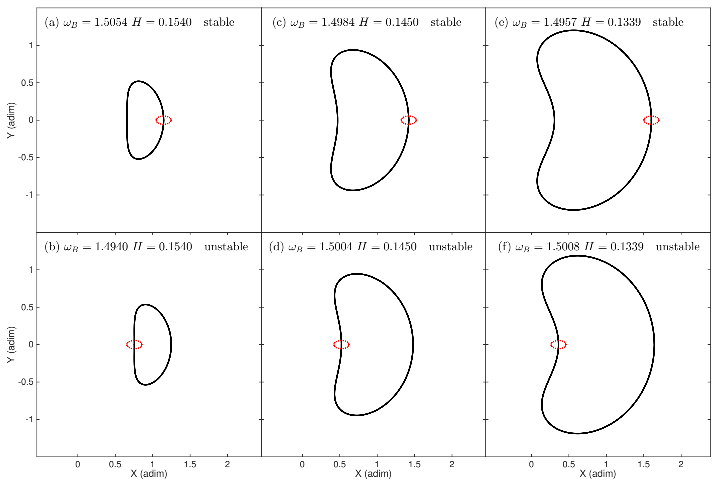

Figure 14: Periodic orbits near the 2 : 3 spin-orbit resonance. The top panel and the bottom panel belong to the right and left branch, respectively. Periodic orbits in the same column have the same total angular momentum.

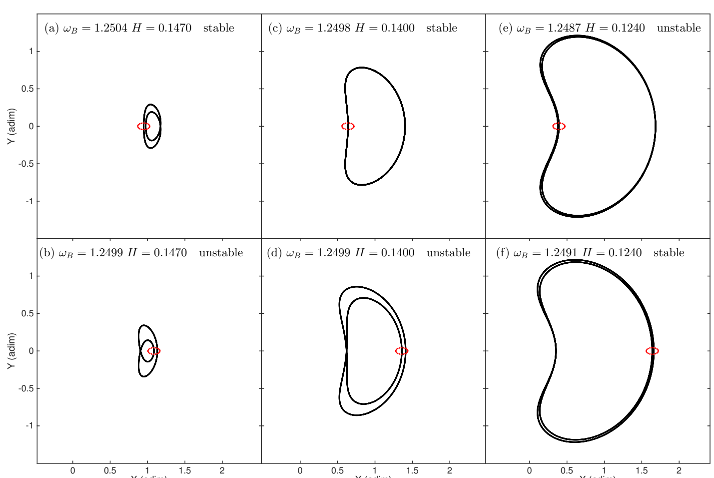

Figure 15: Periodic orbits near the 4 : 5 spin-orbit resonance. The top panel and the bottom panel belong to the right and left branch, respectively. Periodic orbits in the same column have the same total angular momentum.

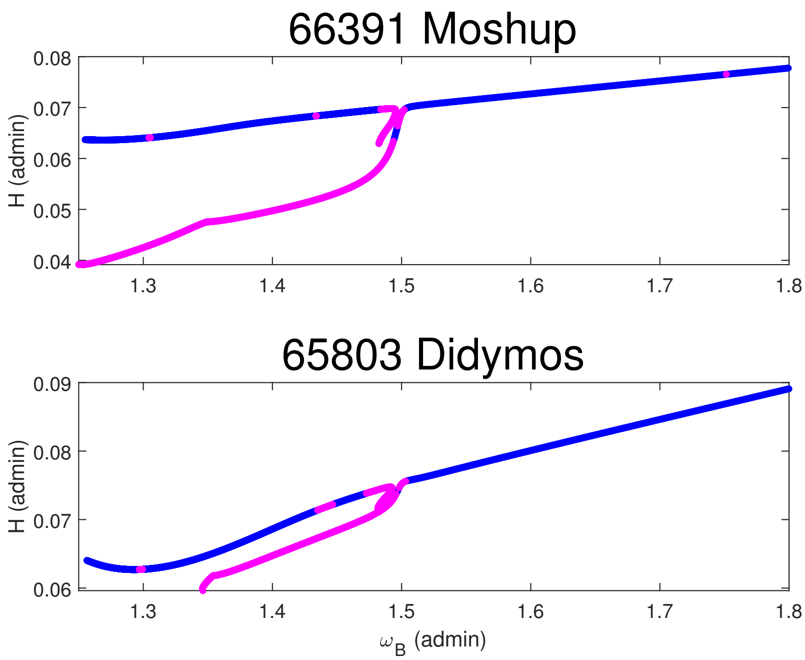

Figure 16: The $H - \omega_B$ curve for the system 66391 Moshup (top) and 65803 Didymos (bottom). The blue and magenta lines indicate that the corresponding periodic orbits are stable and unstable, respectively.

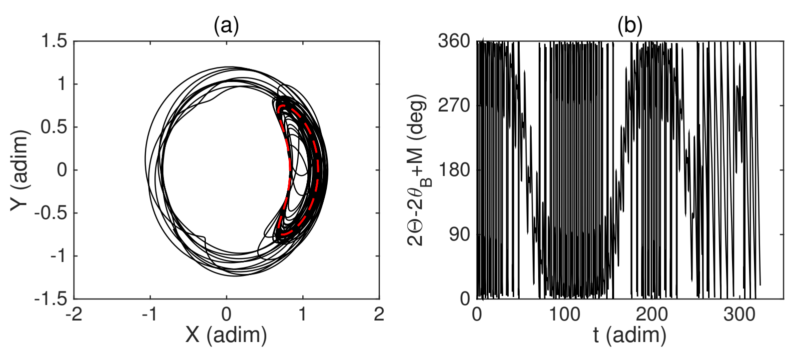

Figure 17: An example of the chaotic rotation of $\mathcal{B}$ near the 2 : 3 spin-orbit resonance in 1999KW4 system. (a) red line: original periodic orbit with $\omega_B = 1.4857$; black line: integrated trajectory for the time span of 25 orbit periods of the original periodic orbit with deviation of 10^{-4} in initial position. (b) time history of the resonance angle $2\Theta - 2\theta_B + M$.

5. Conclusions

The stability of the PF2BP where the rotation is coupled with orbital motion is studied. Different from previous studies which mainly focus on the spin-orbit coupling of the secondary and adopt the assumption of invariant orbit, the current study mainly focuses on the high-order spin-orbit resonances of the primary in a binary asteroid system. We found that there is a contradiction between the results of the full dynamics of the PF2BP and the results by the traditional approach of assuming an invariant mutual orbit. It indicates that the influence on the orbital motion by the rotational motion is non-negligible. In the body-fixed frame of the secondary $\mathcal{A}$, depending on the rotational state of $\mathcal{B}$, totally two kinds of periodic trajectories that the primary $\mathcal{B}$ follows are studied in this work. One kind of periodic family has orbits, not in spin-orbit resonances (called as near-circular families in this work), and the other kind has orbits in spin-orbit resonances (called as resonance families in this work). In the unperturbed cases the resonance families bifurcate from the two near-circular families. In the case, the near-circular family breaks into pieces at the resonance families. The resonance families join with these pieces to form a series of new periodic families. Moreover, in the presence of perturbations, each first-order spin-orbit resonance splits into two branches, with a different configuration of the spin-orbit resonance for each branch. For small to moderate orbit eccentricities, one branch is stable, and the other branch is unstable. Zoomed into the 2:3 spin-orbit, the stable one has moderate orbit eccentricities and large mutual distance. Both two branches have a lower angular momentum in resonance areas. For large perturbations, usually, both branches become unstable and the BAS breaks in these resonances.

6. Discussion

For near-Earth binary asteroid systems, the secondary usually first enters a synchronous rotation state due to tidal dissipations [38], but the primary is not. Under the influence of tidal dissipations or the thermal effect, the rotation rate of the primary may change, becoming slower or faster and crossing a series of spin-orbit resonances. [26] also find a case by numerical integration, in which the synchronous state of BAS breaks when the BAS is near resonance areas. This mechanism prevents the formation of the asteroid pairs with a slow-rotation primary. Some of these asteroid pairs with low-angular momentum are unexpected in existing theories such as (49791) 1999 XF31 et al [39]. However, we found stable branches in small perturbation cases for the families of periodic orbits, which have moderate eccentricities, considerable mutual distance, and low angular momentum. These results provide a possible dynamical path for forming these asteroid pairs where two components of the BAS with near-sphere shapes enter into some spin-orbit resonance along stable branches and become the asteroid pair.

CRediT authorship contribution statement

Hai-Shuo Wang: Software, Formal analysis, Visualization, Writing - Original Draft. **Xiaosheng Xin:** Investigation, Validation, Supervision, Writing - Review & Editing,Visualization. **Xiyun Hou:** Conceptualization, Resources, Writing - Review & Editing, Supervision. **Jinglang Feng:** Investigation.

Declaration of competing interest

The authors declare that they have no known competing financial interests or personal relationships that could haveappeared to influence the work reported in this paper.

Acknowledgement

X.Y.H. wishes to thank the support from National Natural Science Foundation of China (No. 11773017).

Appendix A. Issues related to the monodromy matrix and associated eigenvalues of the periodic orbit

The expression for $A_{8\times8}$ in equation (15) is

$$A_{8\times8} = \begin{pmatrix} 0 & 0 & 0 & 0 & 1 & 0 & 0 & 0 \\ 0 & 0 & 0 & 0 & 0 & 1 & 0 & 0 \\ 0 & 0 & 0 & 0 & 0 & 0 & 1 & 0 \\ 0 & 0 & 0 & 0 & 0 & 0 & 0 & 1 \\ a_{51} & a_{52} & a_{53} & 0 & 0 & a_{56} & 0 & a_{58} \\ a_{61} & a_{62} & a_{63} & 0 & a_{65} & a_{66} & 0 & a_{68} \\ a_{71} & a_{72} & a_{73} & 0 & 0 & 0 & 0 & 0 \\ a_{81} & a_{82} & 0 & 0 & 0 & 0 & 0 & 0 \end{pmatrix} \tag{A.1}$$

in which

$$\begin{aligned}
a_{51} &= \left(\dot{\theta} + \dot{\theta}_A\right)^2 + \frac{2}{S^3} + \frac{12}{S^5}(A_1 + A_2\cos 2\theta + A_3\cos 2\delta), \\
a_{52} &= \frac{6}{S^4}\left(A_2\sin 2\theta + A_3\sin 2\delta\right), \\
a_{53} &= -\frac{6}{S^4}A_3\sin 2\delta, \\
a_{56} &= a_{58} = 2S\left(\dot{\theta} + \dot{\theta}_A\right), \\
a_{61} &= 2\frac{\dot{S}}{S^2}\left(\dot{\theta} + \dot{\theta}_A\right) + \frac{10}{S^6}\left(A_2\sin 2\theta + A_3\sin 2\delta\right) + \frac{6mA_2}{I_z^A}\frac{\sin 2\theta}{S^4}, \\
a_{62} &= -\frac{4}{S^5}\left(A_2\cos 2\theta + A_3\cos 2\delta\right) - \frac{4mA_2}{I_z^A}\frac{\cos 2\theta}{S^3}, \\
a_{63} &= \frac{4}{S^5}A_3\cos 2\delta, \\
a_{65} &= -\frac{2}{S}\left(\dot{\theta} + \dot{\theta}_A\right), \\
a_{66} &= a_{68} = -\frac{2\dot{S}}{S}, \\
a_{71} &= \frac{6mA_2}{I_z^A}\frac{\sin 2\theta}{S^4} - \frac{6mA_3}{I_z^B}\frac{\sin 2\delta}{S^4}, \\
a_{72} &= \frac{4mA_3}{I_z^B}\frac{\cos 2\delta}{S^3} - \frac{4mA_2}{I_z^A}\frac{\cos 2\theta}{S^3}, \\
a_{73} &= -\frac{4mA_3}{I_z^B}\frac{\cos 2\delta}{S^3},
\end{aligned}$$

$$a_{81} = -\frac{6mA_2}{I_z^A}\frac{\sin 2\theta}{S^4},$$
$$a_{82} = \frac{4mA_2}{I_z^A}\frac{\cos 2\theta}{S^3}.$$

The STM mapped over one orbit period T, $\Phi_{8\times 8}(T)$, takes the form

$$\Phi_{8\times 8}(T) = \begin{pmatrix} b_{11} & b_{12} & b_{13} & 0 & b_{15} & b_{16} & b_{17} & b_{18} \\ b_{21} & b_{22} & b_{23} & 0 & b_{25} & b_{26} & b_{27} & b_{28} \\ b_{31} & b_{32} & b_{33} & 0 & b_{35} & b_{36} & b_{37} & b_{38} \\ b_{41} & b_{42} & b_{43} & 1 & b_{45} & b_{46} & b_{47} & b_{48} \\ b_{51} & b_{52} & b_{53} & 0 & b_{55} & b_{56} & b_{57} & b_{58} \\ b_{61} & b_{62} & b_{63} & 0 & b_{65} & b_{66} & b_{67} & b_{68} \\ b_{71} & b_{72} & b_{73} & 0 & b_{75} & b_{76} & b_{77} & b_{78} \\ b_{81} & b_{82} & b_{83} & 0 & b_{85} & b_{86} & b_{87} & b_{88} \end{pmatrix}, \tag{A.2}$$

i.e., the elements in the fourth column all equal zero except the diagonal element, which is unity. This is easy to understand since θ_A does not appear explicitly in equation (8). There should always be on pair of eigenvalues equal to 1 for $\Phi_{8\times 8}(T)$ due to the periodicity condition. In addition, because of the unique structure of $\Phi_{8\times 8}(T)$, it is evident that $\lambda_0 = 1$ is also an eigenvalue of $\Phi_{8\times 8}(T)$ with

$$\boldsymbol{u}^{\lambda_0} = (0,0,0,1,0,0,0,0)^T$$

as the corresponding unit eigenvector. Thus another eigenvalue $\lambda_0' = 1$ also exists according to the properties of the Hamiltonian system. However, due to limited accuracy of the computer, numerical computation of the eigenvalues of $\Phi_{8\times 8}(T)$, such as using `DGEEV` routine of Linear Algebra PACKage (LAPACK), may not produce this one pair of eigenvalues exactly equal to one.

To overcome this problem, we remove the forth row and column from $\Phi_{8\times 8}(T)$

to obtain

$$\mathbf{M}_{7\times 7} = \begin{pmatrix} b_{11} & b_{12} & b_{13} & b_{15} & b_{16} & b_{17} & b_{18} \\ b_{21} & b_{22} & b_{23} & b_{25} & b_{26} & b_{27} & b_{28} \\ b_{31} & b_{32} & b_{33} & b_{35} & b_{36} & b_{37} & b_{38} \\ b_{51} & b_{52} & b_{53} & b_{55} & b_{56} & b_{57} & b_{58} \\ b_{61} & b_{62} & b_{63} & b_{65} & b_{66} & b_{67} & b_{68} \\ b_{71} & b_{72} & b_{73} & b_{75} & b_{76} & b_{77} & b_{78} \\ b_{81} & b_{82} & b_{83} & b_{85} & b_{86} & b_{87} & b_{88} \end{pmatrix}, \tag{A.3}$$

and solve $\mathbf{M}_{7\times 7}$ for the eigenvalues.

Appendix B. 4th order EOMs

$$U = -m\left[\frac{1}{S} + \frac{1}{S^3}\tilde{U}_2 + \frac{1}{S^5}\tilde{U}_4\right], \tag{B.1}$$

$$\tilde{U}_2 = A_1 + A_2\cos 2\theta + A_3\cos 2\delta \tag{B.2}$$

$$\begin{aligned}\tilde{U}_4 =& B_1 + B_2\cos 2\theta + B_3\cos 4\theta + B_4\cos 2\delta + B_5\cos 4\delta \\ &+ B_6\cos 2\phi + B_7\cos(2\theta + 2\delta)\end{aligned} \tag{B.3}$$

$$\frac{\partial U}{\partial S} = m\left[\frac{1}{S^2} + \frac{3}{S^4}\tilde{U}_2 + \frac{5}{S^6}\tilde{U}_4\right] \tag{B.4}$$

$$\frac{\partial U}{\partial \theta} = -m\left[\frac{1}{S^3}\frac{\partial \tilde{U}_2}{\partial \theta} + \frac{1}{S^5}\frac{\partial \tilde{U}_4}{\partial \theta}\right] \tag{B.5}$$

$$\frac{\partial U}{\partial \phi} = -m\left[\frac{1}{S^3}\frac{\partial \tilde{U}_2}{\partial \phi} + \frac{1}{S^5}\frac{\partial \tilde{U}_4}{\partial \phi}\right] \tag{B.6}$$

$$\frac{\partial \tilde{U}_2}{\partial \theta} = -2A_2\sin 2\theta - 2A_3\sin 2\delta \tag{B.7}$$

$$\begin{aligned}\frac{\partial \tilde{U}_4}{\partial \theta} =& -2B_2\sin 2\theta - 4B_3\sin 4\theta - 2B_4\sin 2\delta - 4B_5\sin 4\delta \\ &- 4B_7\sin(2\theta + 2\delta)\end{aligned} \tag{B.8}$$

$$\frac{\partial \tilde{U}_2}{\partial \phi} = 2A_3 \sin 2\delta \tag{B.9}$$

$$\frac{\partial \tilde{U}_4}{\partial \phi} = 2B_4 \sin 2\delta + 4B_5 \sin 4\delta - 2B_6 \sin 2\phi + 2B_7 \sin(2\theta + 2\delta) \tag{B.10}$$

$$\begin{aligned}
a_{51} &= \left(\dot{\theta} + \dot{\theta}_A\right)^2 - \frac{1}{m}\frac{\partial^2 U}{\partial S^2}, \\
a_{52} &= -\frac{1}{m}\frac{\partial^2 U}{\partial S \partial \theta}, \\
a_{53} &= -\frac{1}{m}\frac{\partial^2 U}{\partial S \partial \phi}, \\
a_{56} &= a_{58} = 2S\left(\dot{\theta} + \dot{\theta}_A\right), \\
a_{61} &= 2\frac{\dot{S}}{S^2}\left(\dot{\theta} + \dot{\theta}_A\right) - \left(\frac{1}{I_z^A} + \frac{1}{mS^2}\right)\frac{\partial^2 U}{\partial S \partial \theta} + \frac{2}{mS^3}\frac{\partial U}{\partial \theta} - \frac{1}{I_z^A}\frac{\partial^2 U}{\partial S \partial \phi}, \\
a_{62} &= -\left(\frac{1}{I_z^A} + \frac{1}{mS^2}\right)\frac{\partial^2 U}{\partial \theta^2} - \frac{1}{I_z^A}\frac{\partial^2 U}{\partial \theta \partial \phi}, \\
a_{63} &= -\left(\frac{1}{I_z^A} + \frac{1}{mS^2}\right)\frac{\partial^2 U}{\partial \theta \partial \phi} - \frac{1}{I_z^A}\frac{\partial^2 U}{\partial \phi^2}, \\
a_{65} &= -\frac{2}{S}\left(\dot{\theta} + \dot{\theta}_A\right), \\
a_{66} &= a_{68} = -\frac{2\dot{S}}{S}, \\
a_{71} &= -\frac{1}{I_z^A}\frac{\partial^2 U}{\partial S \partial \theta} - \left(\frac{1}{I_z^A} + \frac{1}{I_z^B}\right)\frac{\partial^2 U}{\partial S \partial \phi}, \\
a_{72} &= -\frac{1}{I_z^A}\frac{\partial^2 U}{\partial \theta^2} - \left(\frac{1}{I_z^A} + \frac{1}{I_z^B}\right)\frac{\partial^2 U}{\partial \theta \partial \phi}, \\
a_{73} &= -\frac{1}{I_z^A}\frac{\partial^2 U}{\partial \theta \partial \phi} - \left(\frac{1}{I_z^A} + \frac{1}{I_z^B}\right)\frac{\partial^2 U}{\partial \phi^2}, \\
a_{81} &= \frac{1}{I_z^A}\left(\frac{\partial^2 U}{\partial S \partial \theta} + \frac{\partial^2 U}{\partial S \partial \phi}\right), \\
a_{82} &= \frac{1}{I_z^A}\left(\frac{\partial^2 U}{\partial \theta^2} + \frac{\partial^2 U}{\partial \theta \partial \phi}\right), \\
a_{83} &= \frac{1}{I_z^A}\left(\frac{\partial^2 U}{\partial \theta \partial \phi} + \frac{\partial^2 U}{\partial \phi^2}\right)
\end{aligned}$$

$$\frac{\partial^2 U}{\partial S^2} = -m\left[\frac{2}{S^3} + \frac{12}{S^5}\tilde{U}_2 + \frac{30}{S^7}\tilde{U}_4\right] \tag{B.11}$$

$$\frac{\partial^2 U}{\partial \theta^2} = -m\left[\frac{1}{S^3}\frac{\partial^2 \tilde{U}_2}{\partial \theta^2} + \frac{1}{S^5}\frac{\partial^2 \tilde{U}_4}{\partial \theta^2}\right] \tag{B.12}$$

$$\frac{\partial^2 U}{\partial \phi^2} = -m\left[\frac{1}{S^3}\frac{\partial^2 \tilde{U}_2}{\partial \phi^2} + \frac{1}{S^5}\frac{\partial^2 \tilde{U}_4}{\partial \phi^2}\right] \tag{B.13}$$

$$\frac{\partial^2 U}{\partial S \partial \theta} = m\left[\frac{3}{S^4}\frac{\partial \tilde{U}_2}{\partial \theta} + \frac{5}{S^6}\frac{\partial \tilde{U}_4}{\partial \theta}\right] \tag{B.14}$$

$$\frac{\partial^2 U}{\partial S \partial \phi} = m\left[\frac{3}{S^4}\frac{\partial \tilde{U}_2}{\partial \phi} + \frac{5}{S^6}\frac{\partial \tilde{U}_4}{\partial \phi}\right] \tag{B.15}$$

$$\frac{\partial^2 U}{\partial \theta \partial \phi} = -m\left[\frac{1}{S^3}\frac{\partial^2 \tilde{U}_2}{\partial \theta \partial \phi} + \frac{1}{S^5}\frac{\partial^2 \tilde{U}_4}{\partial \theta \partial \phi}\right] \tag{B.16}$$

$$\frac{\partial^2 \tilde{U}_2}{\partial \theta^2} = -4A_2 \cos 2\theta - 4A_3 \cos 2\delta \tag{B.17}$$

$$\begin{aligned}\frac{\partial^2 \tilde{U}_4}{\partial \theta^2} =& -4B_2 \cos 2\theta - 16B_3 \cos 4\theta - 4B_4 \cos 2\delta \\ & - 16B_5 \cos 4\delta - 16B_7 \cos(2\theta + 2\delta)\end{aligned} \tag{B.18}$$

$$\frac{\partial^2 \tilde{U}_2}{\partial \phi^2} = -4A_3 \cos 2\delta \tag{B.19}$$

$$\frac{\partial^2 \tilde{U}_4}{\partial \phi^2} = -4B_4 \cos 2\delta - 16B_5 \cos 4\delta - 4B_6 \cos 2\phi - 4B_7 \cos(2\theta + 2\delta) \tag{B.20}$$

$$\frac{\partial^2 \tilde{U}_2}{\partial \theta \partial \phi} = 4A_3 \cos 2\delta \tag{B.21}$$

$$\frac{\partial^2 \tilde{U}_4}{\partial \theta \partial \phi} = 4B_4 \cos 2\delta + 16B_5 \cos 4\delta + 8B_7 \cos(2\theta + 2\delta) \tag{B.22}$$

References

[1] L.-S. Wang, P. S. Krishnaprasad, J. H. Maddocks, Hamiltonian dynamics of a rigid body in a central gravitational field, Celest. Mech. Dyn. Astron. 50 (1991) 349–386.

[2] A. J. Maciejewski, Reduction, relative equilibria and potential in the two rigid bodies problem, Celest. Mech. Dyn. Astron. 63 (1) (1995) 1–28.

[3] H. Kinoshita, Stationary Motions of a Triaxial Body and Their Stabilities, Publications of the Astronomical Society of Japan 24 (1972) 409.

[4] D. Scheeres, Stability in the full two-body problem, Celest. Mech. Dyn. Astron. 83 (1) (2002) 155–169.

[5] W.-S. Koon, J. E. Marsden, S. D. Ross, M. Lo, D. J. Scheeres, Geometric Mechanics and the Dynamics of Asteroid Pairs, in: E. Belbruno, D. Folta, P. Gurfil (Eds.), Astrodynamics, Space Missions, and Chaos, Vol. 1019 of Annals of the New York Academy of Sciences, 2004, p. 11.

[6] H. Cendra, J. E. Marsden, Geometric mechanics and the dynamics of asteroid pairs, Dynamical Systems 20 (1) (2005) 3–21.

[7] K. B. Bhatnagar, U. Gupta, The existence and stability of the equilbrium points of a triaxial rigid body moving around another triaxial rigid body, Celestial Mechanics 39 (1986) 67–83. doi:10.1007/BF01232289.

[8] D. J. Scheeres, Relative Equilibria for General Gravity Fields in the Sphere-Restricted Full 2-Body Problem, Celest. Mech. Dyn. Astron. 94 (2006) 317–349. doi:10.1007/s10569-005-6182-2.

[9] J. Bellerose, D. J. Scheeres, Energy and stability in the Full Two Body Problem, Celest. Mech. Dyn. Astron. 100 (2008) 63–91. doi:10.1007/s10569-007-9108-3.

[10] D. J. Scheeres, Stability of the planar full 2-body problem, Celest. Mech. Dyn. Astron. 104 (2009) 103–128. doi:10.1007/s10569-009-9184-7.

[11] C. D. Murray, S. F. Dermott, Solar system dynamics, Cambridge university press, 1999.

[12] P. Goldreich, S. Peale, Spin-orbit coupling in the solar system, The Astronomical Journal 71 (1966) 425. doi:10.1086/109947.

[13] A. C. Correia, J. Laskar, Mercury's capture into the 3/2 spin–orbit resonance including the effect of core–mantle friction, Icarus 201 (1) (2009) 1–11. doi:https://doi.org/10.1016/j.icarus.2008.12.034.
URL https://www.sciencedirect.com/science/article/pii/S0019103508004429

[14] J. Wisdom, S. J. Peale, F. Mignard, The chaotic rotation of Hyperion, Icarus 58 (1984) 137–152. doi:10.1016/0019-1035(84)90032-0.

[15] A. Celletti, Analysis of resonances in the spin-orbit problem in celestial mechanics - The synchronous resonance., Zeitschrift Angewandte Mathematik und Physik 41 (1990) 174–204. doi:10.1007/BF00945107.

[16] A. Celletti, Analysis of resonances in the spin-orbit problem in celestial mechanics. II - Higher order resonances and some numerical experiments, Zeitschrift Angewandte Mathematik und Physik 41 (1990) 453–479. doi:10.1007/BF00945951.

[17] J. Bellerose, D. J. Scheeres, General dynamics in the Restricted Full Three Body Problem, Acta Astronautica 62 (2008) 563–576. doi:10.1016/j.actaastro.2008.01.018.

[18] D. J. Scheeres, Rotational fission of contact binary asteroids, Icarus 189 (2007) 370–385. doi:10.1016/j.icarus.2007.02.015.

[19] P. Tricarico, M. Sykes, The dynamical environment of dawn at vesta, Planetary and Space Science 58 (12) (2010) 1516–1525. doi:https://doi.org/10.1016/j.pss.2010.07.017.
URL https://www.sciencedirect.com/science/article/pii/S0032063310002199

[20] S. P. Naidu, J.-L. Margot, Near-earth asteroid satellite spins under spin–orbit coupling, The Astronomical Journal 149 (2) (2015) 80.
URL http://stacks.iop.org/1538-3881/149/i=2/a=80

[21] M. Jafari Nadoushan, N. Assadian, Geography of the rotational resonances and their stability in the ellipsoidal full two body problem, Icarus 265 (2016) 175–186. doi:10.1016/j.icarus.2015.10.011.

[22] X. Hou, X. Xin, A Note on the Spin-Orbit, Spin-Spin, and Spin-Orbit-Spin Resonances in the Binary Minor Planet System, The Astronomical Journal 154 (6) (2017) 257. doi:10.3847/1538-3881/aa96ab.

[23] X. Hou, D. J. Scheeres, X. Xin, Mutual potential between two rigid bodies with arbitrary shapes and mass distributions, Celest. Mech. Dyn. Astron. 127 (3) (2017) 369–395. doi:10.1007/s10569-016-9731-y.
URL http://dx.doi.org/10.1007/s10569-016-9731-y

[24] K. Batygin, A. Morbidelli, Spin-Spin Coupling in the Solar System, The Astrophysical Journal 810 (2015) 110. arXiv:1508.00616, doi:10.1088/0004-637X/810/2/110.

[25] H. S. Wang, X. Y. Hou, On the secondary's rotation in a synchronous binary asteroid, Monthly Notices of the Royal Astronomical Society 493 (1) (2020) 171–183. arXiv:https://academic.oup.com/mnras/article-pdf/493/1/171/32468370/staa133.pdf, doi:10.1093/mnras/staa133.
URL https://doi.org/10.1093/mnras/staa133

[26] H.-S. Wang, X.-Y. Hou, Break-up of the synchronous state of binary asteroid systems, Monthly Notices of the Royal Astronomical Society 505 (4) (2021) 6037–6050. arXiv:https://academic.oup.com/mnras/article-pdf/505/4/6037/38873517/stab1585.pdf, doi:10.1093/mnras/stab1585.
URL https://doi.org/10.1093/mnras/stab1585

[27] G. Balmino, Gravitational potential harmonics from the shape of an homogeneous body, Celest. Mech. Dyn. Astron. 60 (1994) 331–364. doi:10.1007/BF00691901.

[28] N. Rambaux, E. Bois, Theory of the Mercury's spin-orbit motion and analysis of its main librations, Astronomy and Astrophysics 413 (2004) 381–393. arXiv:astro-ph/0306387, doi:10.1051/0004-6361:20031446.

[29] S. Breiter, B. Melendo, P. Bartczak, I. Wytrzyszczak, Synchronous motion in the Kinoshita problem. Application to satellites and binary asteroids, Astronomy and Astrophysics 437 (2005) 753–764. doi:10.1051/0004-6361:20053031.

[30] L. Chappaz, K. C. Howell, Exploration of bounded motion near binary systems comprised of small irregular bodies, Celest. Mech. Dyn. Astron. 123 (2) (2015) 123–149.

[31] X. Y. Hou, X. Xin, J. Tang, L. Liu, Dynamics around Libration Points in the Binary Asteroid System, in: 25th International Space Symposium on Flight Dynamics, 2015, p. 140.

[32] G. Gómez, J. Masdemont, J. Mondelo, Dynamical substitutes of the libration points for simplified solar system models, in: Libration Point Orbits and Applications, World Scientific Publishing Company, 2003, pp. 373–397.

[33] X. Y. Hou, L. Liu, On quasi-periodic motions around the triangular libration points of the real Earth-Moon system, Celest. Mech. Dyn. Astron. 108 (2010) 301–313. doi:10.1007/s10569-010-9305-3.

[34] X. Y. Hou, X. Xin, D. J. Scheeres, J. Wang, Stable motions around triangular libration points in the real Earth-Moon system, Monthly Notices of the Royal Astronomical Society 454 (2015) 4172–4181. doi:10.1093/mnras/stv2216.

[35] S. J. Ostro, J.-L. Margot, L. A. M. Benner, J. D. Giorgini, D. J. Scheeres, E. G. Fahnestock, S. B. Broschart, J. Bellerose, M. C. Nolan, C. Magri,

P. Pravec, P. Scheirich, R. Rose, R. F. Jurgens, E. M. De Jong, S. Suzuki, Radar imaging of binary near-earth asteroid (66391) 1999 kw4, Science 314 (5803) (2006) 1276–1280. doi:10.1126/science.1133622.

[36] E. G. Fahnestock, D. J. Scheeres, Simulation and analysis of the dynamics of binary near-Earth Asteroid (66391) 1999 KW4, Icarus 194 (2008) 410–435. doi:10.1016/j.icarus.2007.11.007.

[37] L. Dell'Elce, N. Baresi, S. Naidu, L. Benner, D. Scheeres, Numerical investigation of the dynamical environment of 65803 didymos, Advances in Space Research 59 (5) (2017) 1304–1320. doi:https://doi.org/10.1016/j.asr.2016.12.018.
URL https://www.sciencedirect.com/science/article/pii/S0273117716307220

[38] J.-L. Margot, P. Pravec, P. Taylor, B. Carry, S. Jacobson, Asteroid Systems: Binaries, Triples, and Pairs, in: P. Michel, F. E. DeMeo, W. F. Bottke (Eds.), Asteroids IV, Univ. Arizona Press, Tucson, 2015, pp. 355–374. doi:10.2458/azu_uapress_9780816532131-ch019.

[39] P. Pravec, P. Fatka, D. Vokrouhlický, P. Scheirich, J. Durech, D. Scheeres, P. Kusnirak, K. Hornoch, A. Galad, D. Pray, Y. N. Krugly, O. Burkhonov, S. A. Ehgamberdiev, J. Pollock, N. Moskovitz, A. Thirouin, J. Ortiz, N. Morales, M. Husarik, R. Y. Inasaridze, J. Oey, D. Polishook, J. Hanus, H. Kucakova, J. Vrastil, J. Vilagi, S. Gajdos, L. Kornos, P. Veres, N. Gaftonyuk, T. Hromakina, A. Sergeyev, I. Slyusarev, V. Ayvazian, W. Cooney, J. Gross, D. Terrell, F. Colas, F. Vachier, S. Slivan, B. Skiff, F. Marchis, K. Ergashev, D.-H. Kim, A. Aznar, M. Serra-Ricart, R. Behrend, R. Roy, F. Manzini, I. Molotov, Asteroid pairs: A complex picture, Icarus 333 (2019) 429–463. doi:https://doi.org/10.1016/j.icarus.2019.05.014.
URL https://www.sciencedirect.com/science/article/pii/S0019103519300260